

1 *Supplement information for*

2 **Atmospheric CO₂ dynamics in a coastal megacity: spatiotemporal
3 patterns, sea-land breeze impacts, and anthropogenic-biogenic
4 emission partitioning**

5 Jinwen Zhang¹, Yongjian Liang², Chenglei Pei², Bo Huang³, Yingyan Huang², Xiufeng Lian^{1,3}, Shaojie
6 Song⁴, Chunlei Cheng¹, Cheng Wu¹, Zhen Zhou¹, Junjie Li⁵, Mei Li^{1*}

7 ¹College of Environment and Climate, Institute of Mass Spectrometry and Atmospheric Environment, Guangdong Provincial
8 Engineering Research Center for Online Source Apportionment System of Air Pollution, Guangdong-Hongkong-Macau Joint
9 Laboratory of Collaborative Innovation for Environmental Quality, Jinan University, Guangzhou 511443, China

10 ²Guangzhou Ecological and Environmental Monitoring Center Station, Guangdong, Guangzhou 510006, China

11 ³Guangzhou Hexin Instrument Co., Ltd., Guangdong, Guangzhou 510530, China

12 ⁴College of Environmental Science and Engineering, Nankai University, Tianjin 300350, China

13 ⁵School of Environment, Beijing Jiaotong University, Beijing 100044, China

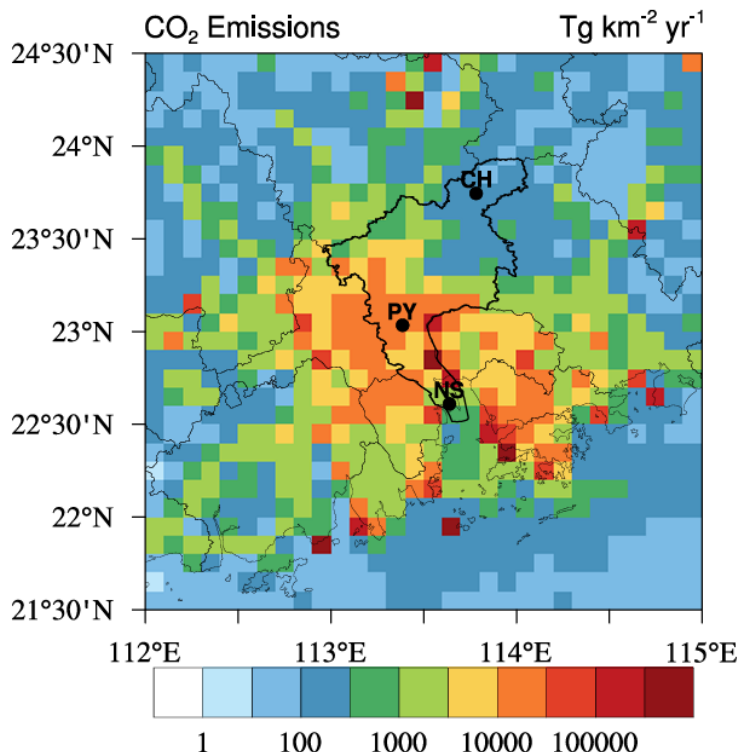
14 *Correspondence to:* Mei Li (limei@jnu.edu.cn)

15 In this document, we describe: (1) site selection strategy; (2) monitoring system and principles of the instruments; (3) wind
16 fields; (4) background concentrations.

17 **1) Site selection strategy**

18 The site selection process for Guangzhou's greenhouse gas monitoring network comprises preliminary screening, precise
19 screening, and field surveys. The preliminary screening phase involves analyzing the city's dominant wind directions,
20 topographic features, and emission distribution to establish a baseline understanding (Fig. S1). Drawing on experiences from
21 other cities and considering local conditions and construction costs, the initial plan proposed three monitoring stations:

- 22 (1) Urban station: located in the densely populated central urban area to monitor atmospheric CO₂ signals driven by
23 anthropogenic emissions.
24 (2) Coastal station: positioned in the southern coastal region to study the impacts of regional transport and coastal-specific
25 weather systems (notably sea-land breezes) on CO₂ concentrations.
26 (3) Suburban station: situated in the northern suburbs to capture CO₂ dynamics under urban ecosystem conditions.



27
28 **Figure S1.** CO₂ emissions in Guangzhou and surrounding cities based on the 2023 EDGAR emission inventory (Crippa et al., 2024).

29 After determining the number of stations, satellite remote sensing was used to identify high-, medium-, and low-CO₂
30 concentration zones. A cluster analysis model screened 5–10 times the proposed number of candidate sites. These candidates
31 were further evaluated using the WRF-STILT model to analyze their sensitivity to CO₂ footprints, ensuring representative and
32 sensitive site selection. Field surveys for final site selection included the following criteria:

- 33 (1) Emission sources: greenhouse gas emission sources within a 1-km radius should be maintained at minimal levels.

- 34 (2) Sampling accessibility: a 360° horizontal capture space around the sampling inlet.
- 35 (3) Geological stability: long-term geological stability to avoid impacts from floods, wildfires, or landslides.
- 36 (4) Infrastructure: minimal electromagnetic interference, stable power supply, lightning protection, and accessible
- 37 communication lines.

- 38 (5) Mobile monitoring: at least one week of mobile greenhouse gas monitoring at each candidate site.

39

40 Priority was given to newly constructed towers or existing open high towers for sampling, as these structures minimize airflow
41 disturbances from supporting frameworks (Verhulst et al., 2017). Towers exceeding 50 meters in height were preferred;
42 however, such platforms account for less than 1 % in Guangzhou and are often located in inaccessible areas. Thus, sites near
43 50 meters were prioritized to ensure well-mixed air sampling and avoid local anthropogenic or natural source-sink influences.

44 **2) Monitoring system**

45 At the inlet front end, hydrophobic PTFE capsule filters and stainless steel tube clamps are installed. The capsule filters remove
46 solid particles larger than 10 μm . Ambient air samples are drawn through 10 mm diameter PTFE-coated black aluminum-
47 plastic tubes via a vacuum pump, with a maximum flow rate of 2 L min⁻¹. Additional filters in the tubing system remove solid
48 particles larger than 2 μm and liquid droplets larger than 0.03 mm. The gas passes through a primary dehumidifier to reduce
49 the dew point temperature to 2–10 °C, preventing condensation in the intake pipes. An ultra-low-temperature automatic
50 cryogenic trap and a multi-channel gas intake system are also installed. Using built-in compressor cooling, the aluminum alloy
51 cryogenic trap can lower the dew point temperature to –50 °C. Optimization of the control program minimizes maintenance
52 requirements for the condensation dehumidifier, ensuring optimal system performance and reducing data artifacts during gas
53 channel switching. Before entering the analyzers, samples pass through the calibration module, where periodic calibration
54 curve establishment and target gas verification ensure measurement precision, accuracy, and long-term stability (detailed in
55 Section 2.3)

56

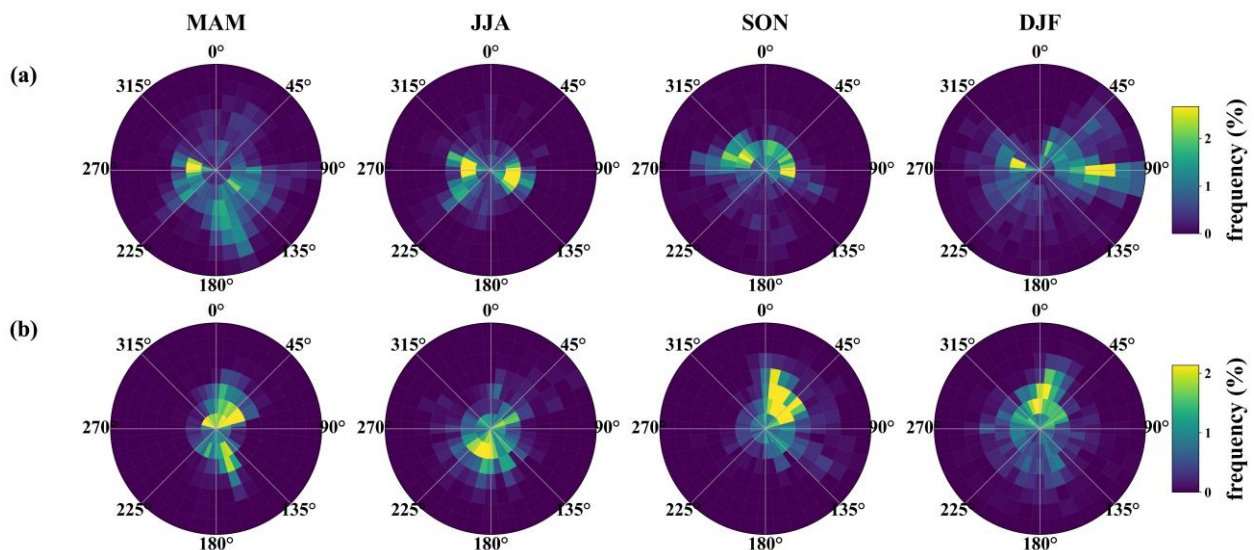
57 The Picarro G2401 greenhouse gas analyzer employs Cavity Ring-Down Spectroscopy (CRDS). Its working principle is based
58 on the near-infrared absorption spectrum unique to greenhouse gases like CO₂. When an infrared laser is reflected by high-
59 reflectivity mirrors within the measurement cavity, the light intensity decays exponentially. The gas concentration is
60 determined by calculating the difference in ring-down time between an empty cavity and one filled with the target gas. The
61 ABB GLA331-GGA greenhouse gas analyzer utilizes Off-Axis Integrated Cavity Output Spectroscopy (OA-ICOS). This
62 technology creates an optical cavity using two highly reflective mirrors, enabling the laser to undergo multiple reflections
63 between them. This amplifies the absorption signal, enhancing measurement sensitivity.

64 3) Wind fields

65 Wind speed and direction are critical indicators of temporal variations in atmospheric CO₂ mole fractions. Figure S2 presents
66 seasonal wind frequency monitoring results for the NS and PY stations, with wind speed resolution of 1.5 m s⁻¹ and directional
67 resolution of 10° :

68 (1) NS Station: average wind speed = 2.86 m s⁻¹. Dominant southerly winds in spring/summer (64 % and 57 % frequency)
69 and northerly winds in autumn/winter (66 % and 56 %).

70 (2) PY Station: average wind speed = 2.12 m s⁻¹. Prevailing northeastern and southeastern winds across seasons.



71
72 **Figure S2.** Observed wind frequency as a function of wind speed and wind direction in spring (MAM), summer (JJA), autumn
73 (SON), and winter (DJF) at NS (a) and PY (b) from January 2023 to September 2024.

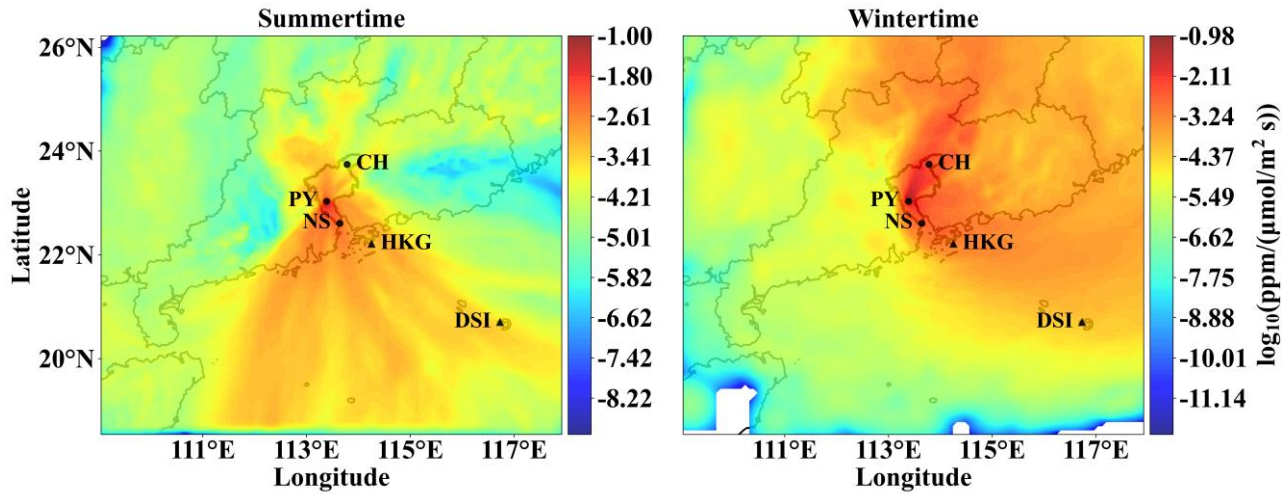
74 4) Background concentrations

75 Real-time monitoring of atmospheric background values entirely unaffected by local sources and sinks in urban areas is
76 challenging. Due to technical and logistical constraints such as site accessibility and power supply, very few monitoring stations
77 are sufficiently remote to remain permanently exposed to pristine air masses (Fang et al., 2015). With urbanization, many
78 regional background stations in suburban areas are increasingly influenced by urban carbon sources, leading to overestimated
79 urban background values (Chen et al., 2024). Here, urban background concentrations are defined as representative values of
80 air masses entering the city from upwind directions, unaffected by local sources or sinks (Verhulst et al., 2017; Mitchell et al.,
81 2018).

82

83 This study combines dominant urban wind patterns, atmospheric transport models, NOAA Earth System Research
84 Laboratory/Global Monitoring Laboratory (NOAA GML) background stations, and Carbon Tracker assimilation data to
85 determine atmospheric CO₂ and CO background values for Guangzhou. Seasonal dominant wind directions at urban stations

86 exhibited similar characteristics (Fig. S2), prompting a focus on summer and winter for airmass origin analysis. Figure S3
 87 illustrates the spatial distribution of average afternoon (12:00–16:00) atmospheric footprints during summer (July) and winter
 88 (December) over Guangzhou. Summer footprints primarily spanned southern urban and marine regions, while winter footprints
 89 extended to northeastern and southeastern urban and marine areas. By tracking air particles entering the city and using samples
 90 from the CO₂ GLOBALVIEWplus v10.1 ObsPack (Schuldt et al., 2024), two NOAA GML background stations—Hok Tsui
 91 (HKG) and Dongsha Island (DSI)—were identified as potential marine background references for Guangzhou. Air particles
 92 from upwind directions passed through both stations in all seasons.



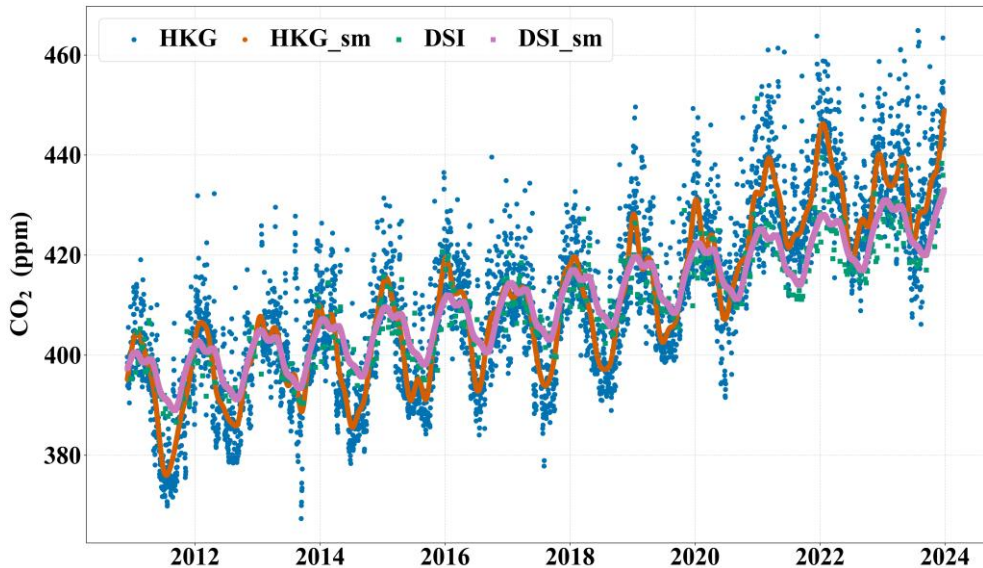
93
 94 **Figure S3.** Spatial distribution of average atmospheric footprints during afternoon hours (12:00–16:00) in summer (July) and winter
 95 (December) based on the PY station.

96 We compared decadal CO₂ time series from these stations (Fig. S4) and applied CCGCRV curve-fitting software for smoothing
 97 (Thoning et al., 1989). HKG data showed significant deviations from smoothed trends, suggesting contamination by local CO₂
 98 surface fluxes. In contrast, DSI data consistently fell within HKG's range, indicating its suitability as Guangzhou's marine
 99 background. For further validation, we compared concentration values from NOAA's CarbonTracker (version CT-NRT.v2024-
 100 5) at grid cells where air particles last resided with DSI observations (Jacobson et al., 2024). During 2023, residuals between
 101 smoothed values were < 2 ppm, with a mean residual of 0.81 ± 0.85 ppm (Fig. S5), confirming DSI's reliability. Due to DSI's
 102 sparse weekly flask sampling, Carbon Tracker data were adopted for marine CO₂ background concentrations. For CO, lacking
 103 Carbon Tracker data, smoothed DSI CO observations served as the urban background reference.

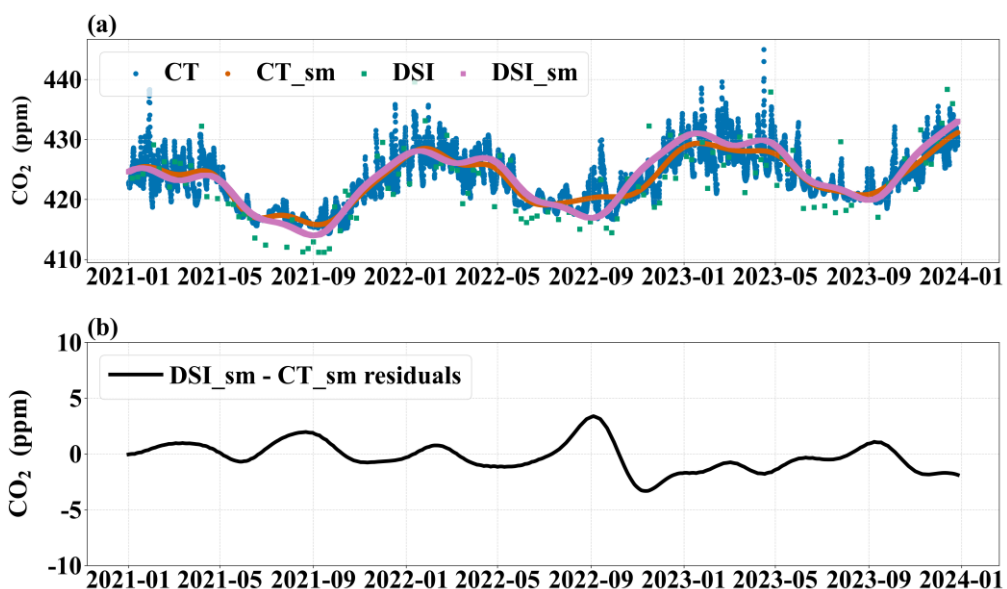
104

105

106



107
108 **Figure S4.** Time series of atmospheric CO₂ concentrations showing both raw monitored data and smoothed values at HKG and DSI
109 stations from November 2, 2010, to December 31, 2023.



110
111 **Figure S5.** (a) Time series of atmospheric CO₂ concentrations showing both raw monitored/simulated data and smoothed values for
112 DSI and Carbon Tracker from January 1, 2021, to December 26, 2023. (b) Residuals between DSI and Carbon Tracker smoothed values.
113
114
115
116
117
118
119

120

121

Table S1 Summary of sea-land breeze day (SLBD) identification methods

Study area	Data	SLBD identification criteria	References
Pearl River Estuary	Observational data	Nighttime offshore winds or calm; ≥ 4 consecutive daytime onshore winds; $\Delta P \leq 5$ hPa; land-sea $\Delta T > 3$ °C	(Qiu and Fan, 2013)
Tianjin	Observational data	≤ 1 isobar line on surface weather maps; land-sea $\Delta T > 0$ °C; ≥ 3 consecutive onshore/offshore winds from sunrise to 2 h post-sunset	(Hao et al., 2017)
West African Coast	Reanalysis & observational data	Offshore/calm winds 6 h before sunrise and 2 h after sunrise; ≥ 2 consecutive onshore winds post-sunrise; $\Delta T > 0$ °C; ≥ 4 h daily sunlight	(Coulibaly et al., 2021)
Zhuhai	Observational data	24 h average wind speed < 10 m s ⁻¹ ; ≥ 3 occurrences of land/sea breeze; absolute wind direction difference between 02:00 and 14:00 = 90–270°	(Zhang et al., 2024)
Pearl River Estuary	Observational data	≤ 1 isobar line at 08:00 and 20:00; ≥ 4 consecutive land/sea breeze hours or ≥ 4 occurrences within 5 consecutive hours; no precipitation 3 h before/after SLB transition	(Mai et al., 2024)
Coastal China	Reanalysis & observational data	24 h average wind speed < 10 m s ⁻¹ ; ≥ 4 consecutive land/sea breeze hours; alternating land-sea breeze cycles within 24 h	(Huang et al., 2025)

122

123

124

125

126

127

128

129

130

131

132

133

134

135

136

137

138

139

140

Table S2 Seasonal temperature averages (°C) at each station

Station	Season	20:00-05:00	09:00-18:00	0:00-23:00
CH	Autumn	23.95	26.12	23.95
	Spring	21.84	23.36	21.84
	Summer	27.80	29.77	27.80
	Winter	14.26	16.07	14.26
PY	Autumn	27.19	28.70	27.19
	Spring	24.18	25.41	24.18
	Summer	30.21	31.67	30.21
	Winter	17.38	18.61	17.38
CH	Autumn	27.57	29.32	27.57
	Spring	24.10	25.10	24.10
	Summer	30.10	31.32	30.10
	Winter	17.91	18.85	17.91

* CH station's temperature measurements were collected from an atmospheric monitoring station 1 km away

141

142

143

144

145

146

147

148

149

150

151

152

153

154

155

156

157

158

159

160

161

162

163

164

165

166

167

168

169

170

171

Table S3 Marine background concentration uncertainties

	Uncertainty estimates	summer	winter
CO ₂ (ppm)	CT _{co2,r}	0.46	0.45
	CT _{co2,s}	0.84	0.54
	BG _{u,co2}	0.96	0.70
CO (ppb)	OBS _{co,r}	2.10	11.79
	OBS _{co,s}	12.50	14.08
	BG _{u,co}	12.68	18.36

172

173

174

175

176

177

178

179

180

181

182

183

184

185

186

187

188

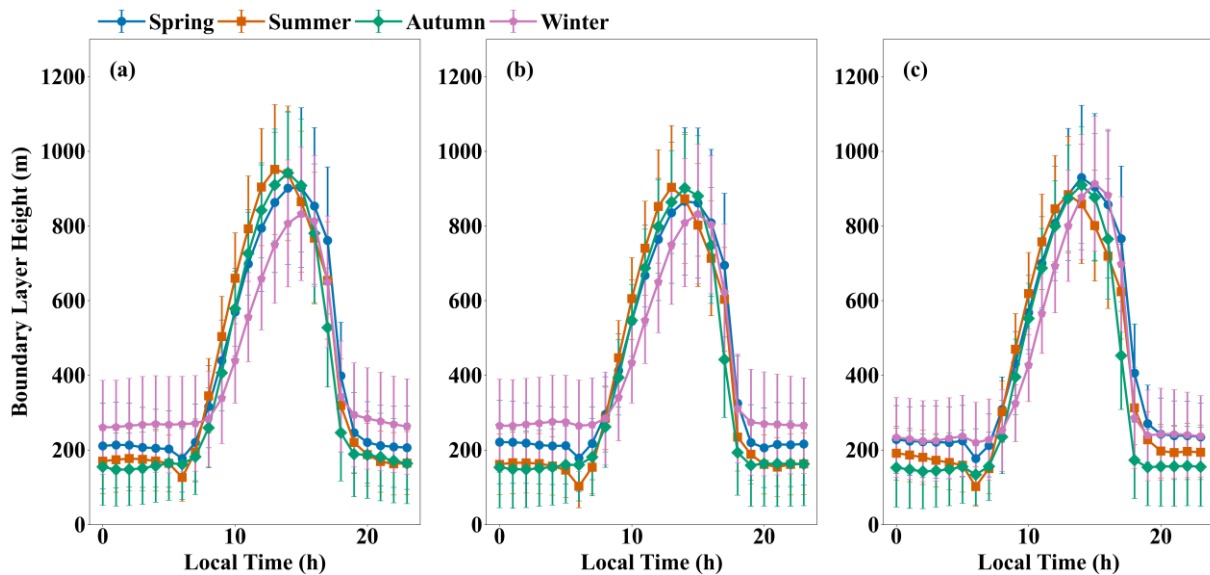
189

190

191

192

193

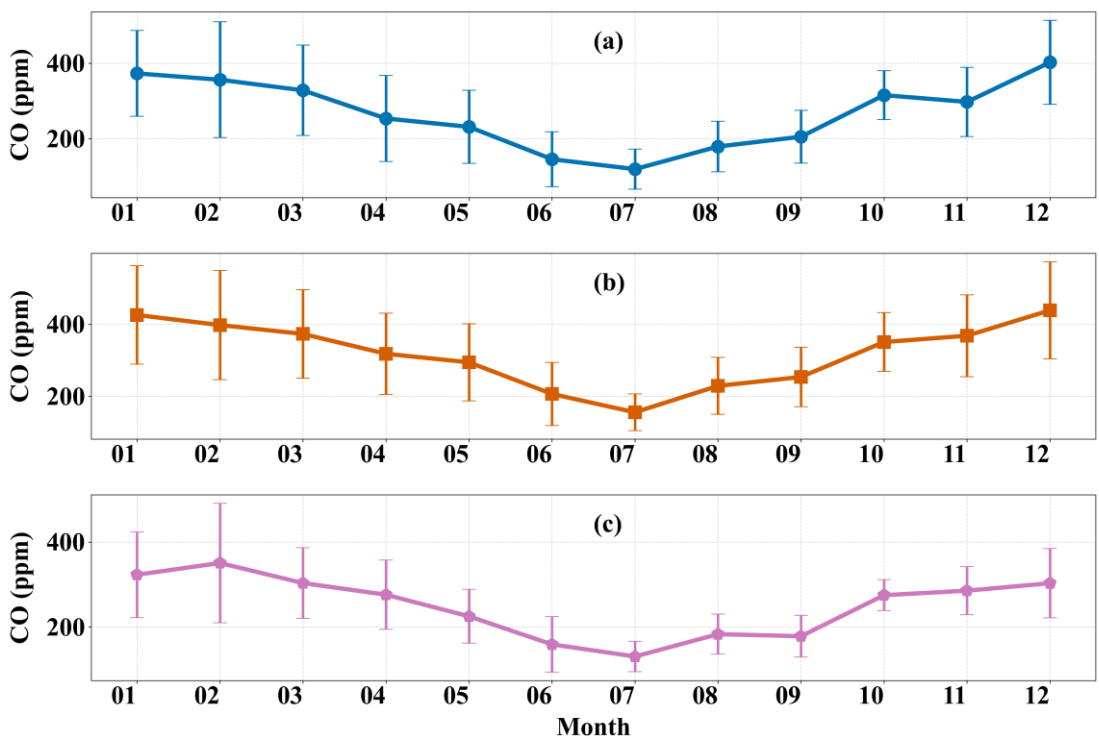


196 **Figure S6.** Diurnal variations in atmospheric boundary layer height at the (a) NS, (b) PY, and (c) CH stations across seasons. The

197 planetary boundary layer height data were obtained from the ERA5 reanalysis product with a spatial resolution of $0.25^\circ \times 0.25^\circ$ (Hersbach,

198 2023). Error bars indicate ± 1 standard deviation (SD).

216

217
218 **Figure S7.** Monthly mean CO concentrations at the (a) NS, (b) PY, and (c) CH stations. Error bars indicate ± 1 SD.
219
220
221
222
223
224
225
226
227
228
229
230
231
232
233
234

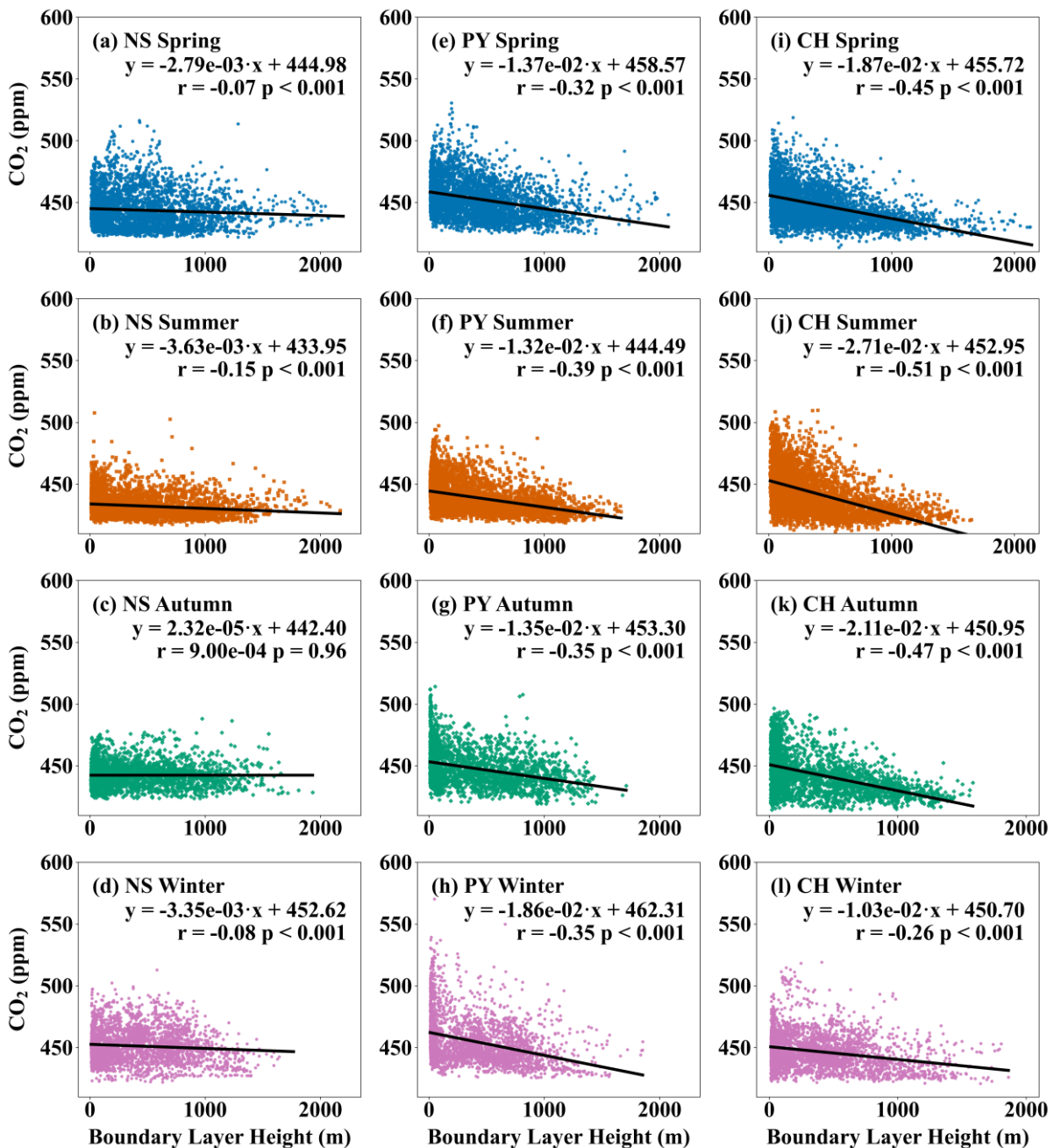
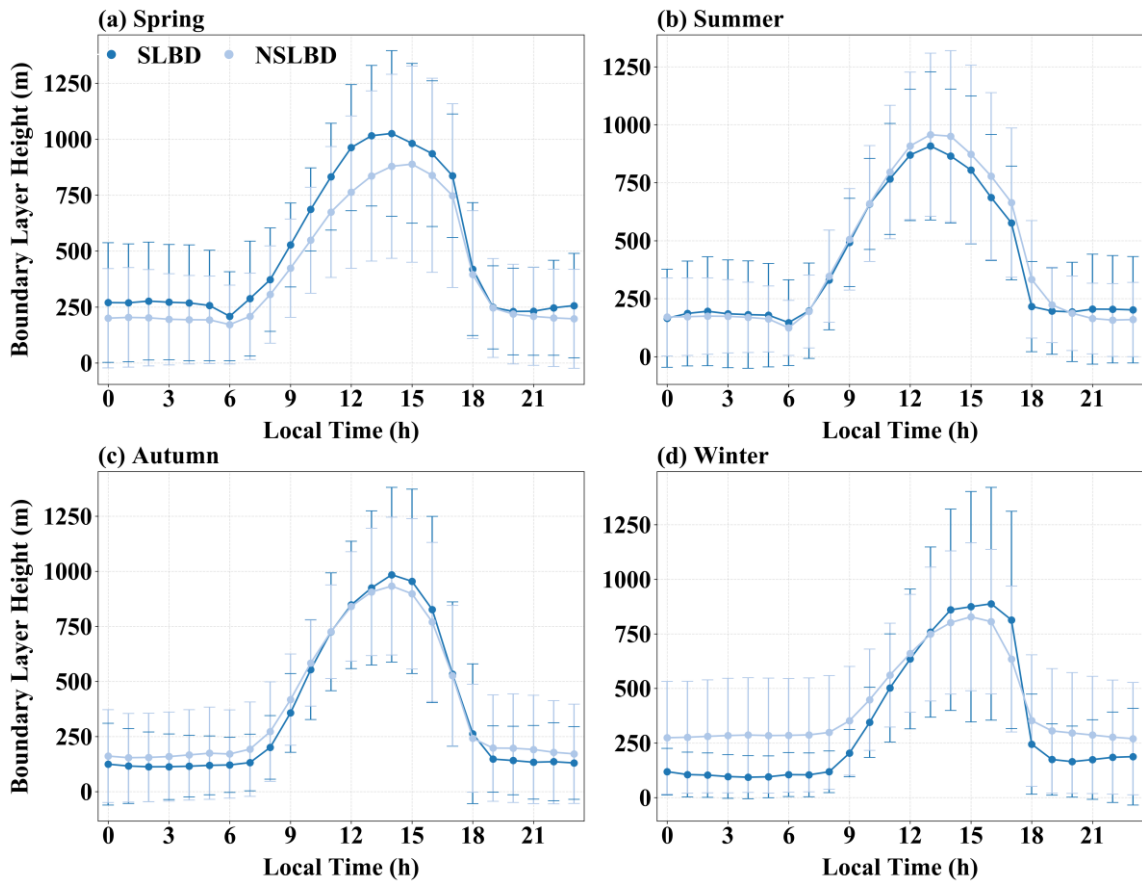


Figure S8. Correlations between atmospheric CO₂ concentrations and boundary layer height at the NS (a–d), PY (e–h), and CH (i–l)

stations across seasons.



248

249 **Figure S9.** Diurnal variations in atmospheric boundary layer height at the NS station during sea-land breeze days (SLBD) and non-SLB
 250 days (NSLBD) across seasons. Error bars indicate ± 1 SD.

251

252

253

254

255

256

257

258

259

260

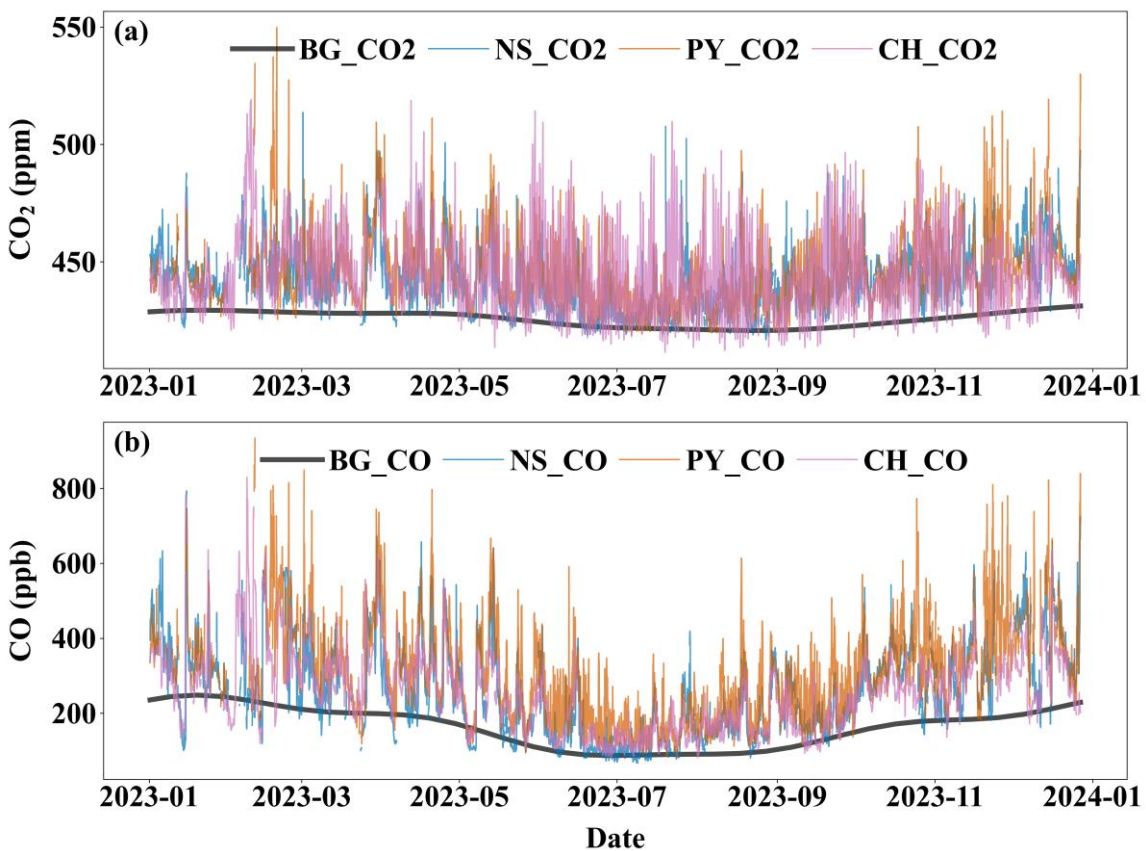
261

262

263

264

265



266

267

Figure S10. Time series of (a) CO₂ and (b) CO concentrations at each station compared with urban marine background levels.

268

269

270

271

272

273

274

275

276

277

278

279

280

281

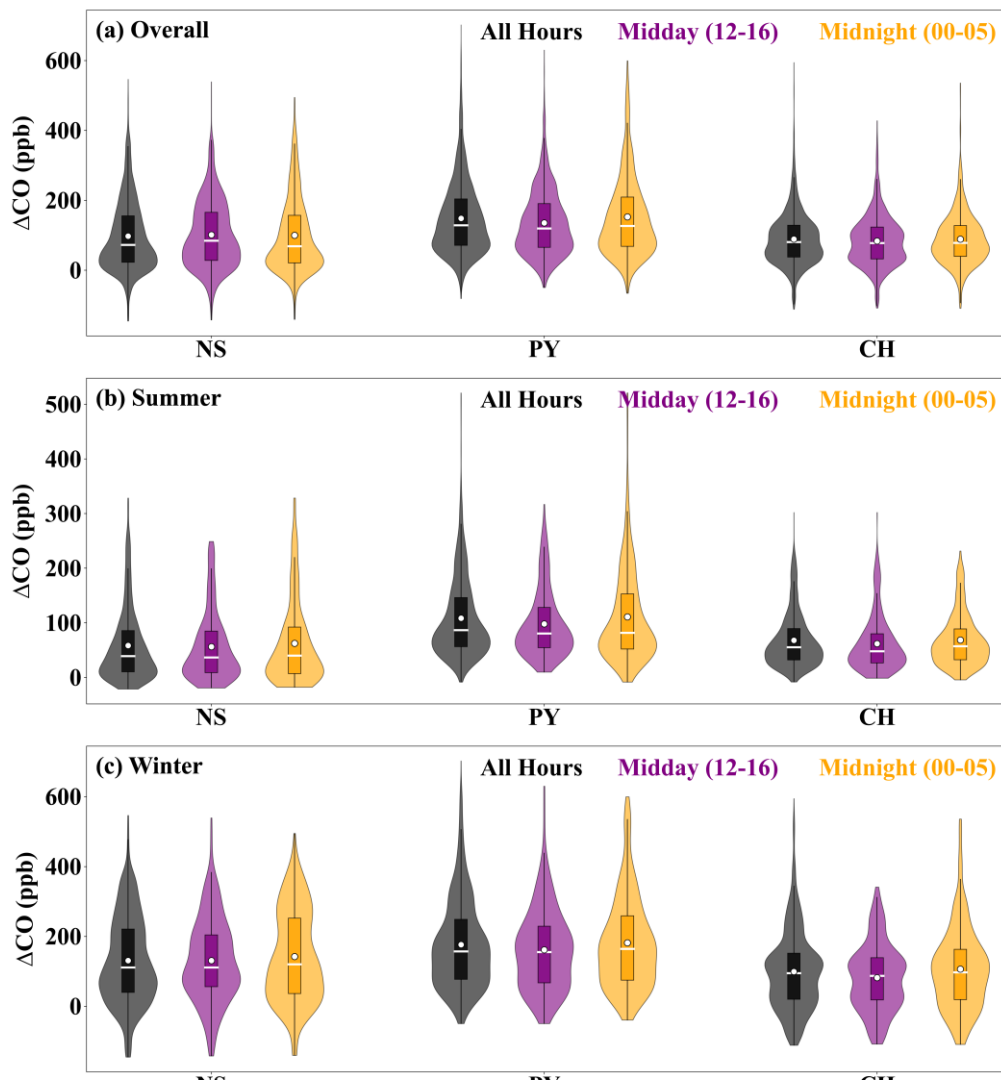
282

283

284

285

286



289 **Figure S11.** Hourly CO enhancement above the marine background level at each station during the (a) overall, (b) summer, and (c) winter
290 periods. The white dots represent the mean values.
291
292
293
294
295
296
297
298

299 **References**

- 300 Chen, Y., Lu, Y., Qi, B., Ma, Q., Zang, K., Lin, Y., Liu, S., Pan, F., Li, S., and Guo, P.: Atmospheric CO₂ in the megacity
301 Hangzhou, China: Urban-suburban differences, sources and impact factors, *Sci. Total Environ.*, 926, 171635,
302 <https://doi.org/10.1016/j.scitotenv.2024.171635>, 2024.
- 303 Coulibaly, A., Omotosho, B. J., Sylla, M. B., Diallo, Y., and Ballo, A.: Numerical simulation of land and sea-breeze (LSB)
304 circulation along the Guinean Coast of West Africa, *Model. Earth Syst. Environ.*, 7, 2031-2045,
305 <https://doi.org/10.1007/s40808-020-00953-0>, 2021.
- 306 Crippa, M., Guizzardi, D., Pagani, F., Banja, M., Muntean, M., Schaaf, E., Monforti-Ferrario, F., Becker, W. E., Quadrelli,
307 R., Risquez Martin, A., Taghavi-Moharamli, P., Köykkä, J., Grassi, G., Rossi, S., Melo, J., Oom, D., Branco, A., San-
308 Miguel, J., Manca, G., Pisoni, E., Vignati, E., and Pekar, F.: GHG emissions of all world countries, Publications Office of
309 the European Union, <https://doi/10.2760/4002897>, 2024.
- 310 Fang, S., Tans, P., Steinbacher, M., Zhou, L., and Luan, T.: Comparison of the regional CO₂ mole fraction filtering
311 approaches at a WMO/GAW regional station in China, *Atmos. Meas. Tech.*, 8, 5301-5313, <https://doi.org/10.5194/amt-8-5301-2015>, 2015.
- 313 Hao, T., Chen, S., Cai, Z., Shan, X., Meng, L., Han, S., and Dong, G.: Influence of sea breeze on atmospheric pollutant
314 concentration over Tianjin, *China Environmental Science*, 37(9), 3247-3257, <https://doi.org/10.3969/j.issn.1000-6923.2017.09.006>, 2017.
- 316 Hersbach, H., Bell, B., Berrisford, P., Biavati, G., Horányi, A., Muñoz Sabater, J., Nicolas, J., Peubey, C., Radu, R., Rozum,
317 I., Schepers, D., Simmons, A., Soci, C., Dee, D., Thépaut, J-N: ERA5 hourly data on single levels from 1940 to present,
318 Copernicus Climate Change Service (C3S) Climate Data Store (CDS) [dataset], <https://10.24381/cds.adbb2d47>, 2023.
- 319 Huang, Y., Li, S., Zhu, Y., Liu, Y., Hong, Y., Chen, X., Deng, W., Xi, X., Lu, X., and Fan, Q.: Increasing sea -land breeze
320 frequencies over coastal areas of China in the past five decades, *Geophys. Res. Lett.*, 52, e2024GL112480,
321 <https://doi.org/10.1029/2024GL112480>, 2025.
- 322 Jacobson, A. R., Schuldt, K. N., Andrews, A., Miller, J. B., Oda, T., Basu, S., Mund, J., Weir, B., Ott, L., Aalto, T., Abshire, J.
323 B., Aikin, K., Allen, G., Andrade, M., Apadula, F., Arnold, S., Baier, B., Bakwin, P., Bartyzel, J., Bentz, G., Bergamaschi,
324 P., Beyersdorf, A., Biermann, T., Biraud, S. C., Blanc, P.-E., Boenisch, H., Bowling, D., Brailsford, G., Brand, W. A.,
325 Brunner, D., Bui, T. P., Burban, B., Bäni, L., Calzolari, F., Chang, C. S., Chen, H., Chen, G., Chmura, L., Clark, S.,
326 Climadat, S., Colomb, A., Commane, R., Condori, L., Conen, F., Conil, S., Couret, C., Cristofanelli, P., Cuevas, E.,
327 Curcoll, R., Daube, B., Davis, K. J., De Mazière, M., De Wekker, S., Dean-Day, J. M., Della Coletta, J., Delmotte, M., Di
328 Iorio, T., DiGangi, E., DiGangi, J. P., Dickerson, R., Elsasser, M., Emmenegger, L., Fang, S., Forster, G., France, J.,
329 Frumau, A., Fuente-Lastra, M., Galkowski, M., Gatti, L. V., Gehrlein, T., Gerbig, C., Gheusi, F., Gloor, E., Goto, D.,
330 Griffis, T., Hammer, S., Hanisco, T. F., Hanson, C., Haszpra, L., Hatakka, J., Heimann, M., Heliasz, M., Heltai, D., Henne,
331 S., Hensen, A., Hermans, C., Hermansen, O., Hintsa, E., Hoheisel, A., Holst, J., Iraci, L. T., Ivakhov, V., Jaffe, D. A.,
332 Jordan, A., Joubert, W., Kang, H.-Y., Karion, A., Kawa, S. R., Kazan, V., Keeling, R. F., Keronen, P., Kim, J., Klausen, J.,
333 Kneuer, T., Ko, M.-Y., Kolari, P., Kominkova, K., Kort, E., Kozlova, E., Krummel, P. B., Kubistin, D., Kulawik, S. S.,
334 Kumps, N., Labuschagne, C., Lam, D. H., Lan, X., Langenfelds, R. L., Lanza, A., Laurent, O., Laurila, T., Lauvaux, T.,
335 Lavric, J., Law, B. E., Lee, C.-H., Lee, J., Lehner, I., Lehtinen, K., Leppert, R., Leskinen, A., Leuenberger, M., Leung, W.
336 H., Levin, I., Levula, J., Lin, J., Lindauer, M., Lindroth, A., Loh, Z. M., Lopez, M., Lunder, C. R., Löfvenius, M. O.,
337 Machida, T., Mammarella, I., Manca, G., Manning, A., Manning, A., Marek, M. V., Marklund, P., Marrero, J. E., Martin,
338 M. Y., Martin, D., Martins, G. A., Matsueda, H., McKain, K., Meijer, H., Meinhardt, F., Merchant, L., Metzger, J.-M.,
339 Mihalopoulos, N., Miles, N. L., Miller, C. E., Mitchell, L., Monteiro, V., Montzka, S., Mooszen, H., Moreno, C., Morgan,
340 E., Morgui, J.-A., Morimoto, S., Munger, J. W., Munro, D., Mutuku, M., Myhre, C. L., Mölder, M., Müller-Williams, J.,
341 Nakaoka, S.-I., Necki, J., Newman, S., Nichol, S., Nisbet, E., Niwa, Y., Njiru, D. M., Noe, S. M., Nojiri, Y., O'Doherty, S.,
342 Obersteiner, F., Paplawsky, B., Parworth, C. L., Peischl, J., Peltola, O., Peters, W., Philippon, C., Piacentino, S., Pichon, J.
343 M., Pickers, P., Piper, S., Pitt, J., Plass-Dülmer, C., Platt, S. M., Prinzivalli, S., Ramonet, M., Ramos, R., Ren, X., Reyes-

- 344 Sanchez, E., Richardson, S. J., Rigouleau, L.-J., Riris, H., Rivas, P. P., Rothe, M., Roulet, Y.-A., Ryerson, T., Ryoo, J.-M.,
345 Sargent, M., Sasakawa, M., Schaefer, H., Scheeren, B., Schmidt, M., Schuck, T., Schumacher, M., Seibel, J., Seifert, T.,
346 Sha, M. K., Shepson, P., Shin, D., Shook, M., Sloop, C. D., Smale, D., Smith, P. D., Spain, G., St. Clair, J. M., Steger, D.,
347 Steinbacher, M., Stephens, B., Sweeney, C., Sørensen, L. L., Taipale, R., Takatsui, S., Tans, P., Thoning, K., Timas, H.,
348 Torn, M., Trisolino, P., Turnbull, J., Vermeulen, A., Viner, B., Vitkova, G., Walker, S., Watson, A., Weiss, R., Weyrauch,
349 D., Wofsy, S. C., Worsey, J., Worthy, D., Xueref-Remy, I., Yates, E. L., Young, D., Yver-Kwok, C., Zaehle, S., Zahn, A.,
350 Zellweger, C., Zimnoch, M., de Souza, R. A., di Sarra, A. G., van Dinther, D., and van den Bulk, P.: CarbonTracker CT-
351 NRT.v2024-5, NOAA Earth System Research Laboratory [dataset], <https://10.15138/atpd-k925>, 2024.
- 352 Mai, J., Yu, L., Deng, T., Wu, D., Qing, P., and Yu, X.: Impact of sea-land breezes on the ozone pollution over the Pearl River
353 Estuary, China Environmental Science, 45(03), 1198-1209, <https://doi.org/10.19674/j.cnki.issn1000-6923.20241102.001>,
354 2024.
- 355 Mitchell, L. E., Lin, J. C., Bowling, D. R., Pataki, D. E., Strong, C., Schauer, A. J., Bares, R., Bush, S. E., Stephens, B. B.,
356 and Mendoza, D.: Long-term urban carbon dioxide observations reveal spatial and temporal dynamics related to urban
357 characteristics and growth, P. Natl. Acad. Sci. USA., 115, 2912-2917, <https://doi.org/10.1073/pnas.170239311>, 2018.
- 358 Qiu, X. and Fan, S.: Study on the application of auto-meteorological station data in local circulations analysis such as the
359 sea-land breeze, Acta Scientiarum Naturalium Universitatis Sunyatseni, 52(2), 133-136,
360 <https://doi.org/10.13471/j.cnki.acta.sonus.2013.02.025>, 2013.
- 361 Schuldt, K. N., Mund, J., Aalto, T., Abshire, J. B., Aikin, K., Allen, G., Andrade, M., Andrews, A., Apadula, F., Arnold, S.,
362 Baier, B., Bakwin, P., Bartyzel, J., Bentz, G., Bergamaschi, P., Beyersdorf, A., Biermann, T., Biraud, S. C., Blanc, P.-E.,
363 Boenisch, H., Bowling, D., Brailsford, G., Brand, W. A., Brunner, D., Bui, T. P., Burban, B., Bäni, L., Calzolari, F., Chang,
364 C. S., Chen, H., Chen, G., Chmura, L., Clark, S., Climadat, S., Colomb, A., Commane, R., Condori, L., Conen, F., Conil,
365 S., Courret, C., Cristofanelli, P., Cuevas, E., Curcoll, R., Daube, B., Davis, K. J., De Mazière, M., De Wekker, S., Dean-
366 Day, J. M., Della Coletta, J., Delmotte, M., Di Iorio, T., DiGangi, E., DiGangi, J. P., Dickerson, R., Elsasser, M.,
367 Emmenegger, L., Fang, S., Forster, G., France, J., Frumau, A., Fuente-Lastra, M., Galkowski, M., Gatti, L. V., Gehrlein,
368 T., Gerbig, C., Gheusi, F., Gloor, E., Goto, D., Griffis, T., Hammer, S., Hanisco, T. F., Hanson, C., Haszpra, L., Hatakka,
369 J., Heimann, M., Heliasz, M., Heltai, D., Henne, S., Hensen, A., Hermans, C., Hermansen, O., Hintsa, E., Hoheisel, A.,
370 Holst, J., Iraci, L. T., Ivakhov, V., Jaffe, D. A., Jordan, A., Joubert, W., Kang, H.-Y., Karion, A., Kawa, S. R., Kazan, V.,
371 Keeling, R. F., Keronen, P., Kim, J., Klausen, J., Kneuer, T., Ko, M.-Y., Kolari, P., Kominkova, K., Kort, E., Kozlova, E.,
372 Krummel, P. B., Kubistin, D., Kulawik, S. S., Kumps, N., Labuschagne, C., Lam, D. H., Lan, X., Langenfelds, R. L.,
373 Lanza, A., Laurent, O., Laurila, T., Lauvaux, T., Lavric, J., Law, B. E., Lee, C.-H., Lee, J., Lehner, I., Lehtinen, K.,
374 Leppert, R., Leskinen, A., Leuenberger, M., Leung, W. H., Levin, I., Levula, J., Lin, J., Lindauer, M., Lindroth, A., Loh, Z.
375 M., Lopez, M., Lunder, C. R., Löfvenius, M. O., Machida, T., Mammarella, I., Manca, G., Manning, A., Manning, A.,
376 Marek, M. V., Marklund, P., Marrero, J. E., Martin, M. Y., Martin, D., Martins, G. A., Matsueda, H., McKain, K., Meijer,
377 H., Meinhardt, F., Merchant, L., Metzger, J.-M., Mihalopoulos, N., Miles, N. L., Miller, C. E., Miller, J. B., Mitchell, L.,
378 Monteiro, V., Montzka, S., Mooszen, H., Moreno, C., Morgan, E., Morgui, J.-A., Morimoto, S., Munger, J. W., Munro, D.,
379 Mutuku, M., Myhre, C. L., Mölder, M., Müller-Williams, J., Nakaoka, S.-I., Necki, J., Newman, S., Nichol, S., Nisbet, E.,
380 Niwa, Y., Njiru, D. M., Noe, S. M., Nojiri, Y., O'Doherty, S., Obersteiner, F., Paplawsky, B., Parworth, C. L., Peischl, J.,
381 Peltola, O., Peters, W., Philippon, C., Piacentino, S., Pichon, J. M., Pickers, P., Piper, S., Pitt, J., Plass-Dülmer, C., Platt, S.
382 M., Prinzivalli, S., Ramonet, M., Ramos, R., Ren, X., Reyes-Sanchez, E., Richardson, S. J., Rigouleau, L.-J., Riris, H.,
383 Rivas, P. P., Rothe, M., Roulet, Y.-A., Ryerson, T., Ryoo, J.-M., Sargent, M., Sasakawa, M., Schaefer, H., Scheeren, B.,
384 Schmidt, M., Schuck, T., Schumacher, M., Seibel, J., Seifert, T., Sha, M. K., Shepson, P., Shin, D., Shook, M., Sloop, C.
385 D., Smale, D., Smith, P. D., Spain, G., St. Clair, J. M., Steger, D., Steinbacher, M., Stephens, B., Sweeney, C., Sørensen,
386 L. L., Taipale, R., Takatsui, S., Tans, P., Thoning, K., Timas, H., Torn, M., Trisolino, P., Turnbull, J., Vermeulen, A.,
387 Viner, B., Vitkova, G., Walker, S., Watson, A., Weiss, R., Weyrauch, D., Wofsy, S. C., Worsey, J., Worthy, D., Xueref-
388 Remy, I., Yates, E. L., Young, D., Yver-Kwok, C., Zaehle, S., Zahn, A., Zellweger, C., Zimnoch, M., de Souza, R. A., di

- 389 Sarra, A. G., van Dinther, D., and van den Bulk, P.: Multi-laboratory compilation of atmospheric carbon dioxide data for
390 the period 1957-2023 (obspack_co2_1_test_GLOBALVIEWplus_v10.1_2024-11-13), NOAA Earth System Research
391 Laboratory, Global Monitoring Laboratory [dataset], <https://doi.org/10.25925/20241101>, 2024.
- 392 Verhulst, K. R., Karion, A., Kim, J., Salameh, P. K., Keeling, R. F., Newman, S., Miller, J., Sloop, C., Pongetti, T., and Rao,
393 P.: Carbon dioxide and methane measurements from the Los Angeles Megacity Carbon Project—Part 1: calibration, urban
394 enhancements, and uncertainty estimates, *Atmos. Chem. Phys.*, 17, 8313-8341, <https://doi.org/10.5194/acp-17-8313-2017>,
395 2017.
- 396 Zhang, L., Lin, J., Shao, Y., Huang, S., Fan, S., and Wei, W.: Understanding the impact of sea and land breezes on ozone
397 pollution in the Pearl River Delta, *Acta Scientiae Circumstantiae*, 44(1), 74-85,
398 <https://doi.org/10.13671/j.hjkxxb.2023.0285>, 2024.
- 399